Resonant SPP modes supported by discrete metal nanoparticles on high-index substrates

F. J. Beck,[1,3,*] E. Verhagen,[2,4] S. Mokkapati,[1] A. Polman,[2] K. R. Catchpole[1]

[1]*Centre for Sustainable Energy Systems, College of Engineering and Computer Science, The Australian National University, Canberra, ACT 0200, Australia*
[2]*Centre for Nanophotonics, FOM Institute AMOLF, Science Park 104, 1098 XG Amsterdam, Netherlands*
[3]*Current address; ICFO-Institut de Ciencies Fotonique, 08860 Castelldefels (Barcelona), Spain*
[4]*Current address: École Polytechnique Fédérale de Lausanne (EPFL), 1015 Lausanne, Switzerland*
**fiona.beck@icfo.es*

Abstract: We provide a new physical interpretation of scattering from plasmonic nanoparticles on high-index substrates. We demonstrate the excitation of different types of resonant modes on disk-shaped, Ag nanoparticles. At short wavelengths, the resonances are localised at the top of the particle, while at longer wavelengths they are localised at the Ag/substrate interface. We attribute the long wavelength resonances to geometric resonances of surface plasmon polaritons (SPPs) at the Ag/substrate interface. We show that particles that support resonant SPP modes have enhanced scattering cross-sections when placed directly on a high-index substrate; up to 7.5 times larger than that of a dipole scatterer with an equivalent free-space resonance. This has implications for designing scattering nanostructures for light trapping solar cells.

OCIS codes: (350.6050) Solar energy; (5403) Plasmonics.

References and links

1. G. Mie, "Beiträge zur Optik trüber Medien, speziell kolloidaler Metallösungen," Ann. Phys. **25**(3), 377–445 (1908).
2. H. A. Atwater, and A. Polman, "Plasmonics for improved photovoltaic devices," Nat. Mater. **9**(3), 205–213 (2010).
3. P. A. Bobbert, and J. Vlieger, "Light scattering by a sphere on a substrate," Phys. Scr. **137A**, 209–--242 (1986).
4. H. Weyl, "Ausbreitung eiektromagnetischer, Wellen uber einem ebenen Leiter," Ann. Phys. **4**(21), 481–500 (1919).
5. Y. A. Akimov, W. S. Koh, and K. Ostrikov, "Enhancement of optical absorption in thin-film solar cells through the excitation of higher-order nanoparticle plasmon modes," Opt. Express **17**(12), 10195–10205 (2009).
6. C. Hägglund, Z. Zach, G. Petersson, and B. Kasemo, "Electromagnetic coupling of light into a silicon solar cell by nanodisk plasmons," Appl. Phys. Lett. **92**(5), 053110 (2008).
7. K. R. Catchpole, and A. Polman, "Design principles for particle plasmon enhanced solar cells," Appl. Phys. Lett. **93**(19), 191113 (2008).
8. Y. A. Akimov, K. Ostrikov, and E. P. Li, "Surface Plasmon Enhancement of Optical Absorption in Thin- Film Silicon Solar Cells," Plasmonics **4**(2), 107–113 (2009).
9. H. R. Stuart, and D. G. Hall, "Enhanced dipole-dipole interaction between elementary radiators near a surface," Phys. Rev. Lett. **80**(25), 5663–5666 (1998).
10. B. J. Soller, and D. G. Hall, "Energy transfer at optical frequencies to silicon-based waveguiding structures," J. Opt. Soc. Am. A **18**(10), 2577–2584 (2001).
11. B. J. Soller, and D. G. Hall, "Scattering enhancement from an array of interacting dipoles near a planar waveguide," J. Opt. Soc. Am. B **19**(10), 2437–2448 (2002).
12. K. R. Catchpole, and S. Pillai, "Absorption enhancement due to scattering by dipoles into silicon waveguides," J. Appl. Phys. **100**(4), 044504–044508 (2006).
13. S. Pillai, K. R. Catchpole, T. Trupke, and M. A. Green, "Surface plasmon enhanced silicon solar cells," J. Appl. Phys. **101**(9), 093105 (2007).
14. S. H. Lim, W. Mar, P. Matheu, D. Derkacs, and E. T. Yu, "Photocurrent spectroscopy of optical absorption enhancement in silicon photodiodes via scattering from surface plasmon polaritons in gold nanoparticles," J. Appl. Phys. **101**(10), 104309 (2007).
15. C. F. Bohren, and D. R. Huffman, *Absorption and scattering of light by small particles* (Wiley- Interscience, New York, 1983).
16. J. Mertz, "Radiative absorption, fluorescence, and scattering of a classical dipole near a lossless interface: a unified description," J. Opt. Soc. Am. B **17**(11), 1906 (2000).

#138671 - $15.00 USD Received 29 Nov 2010; revised 21 Jan 2011; accepted 21 Jan 2011; published 4 Feb 2011

17. F. J. Beck, S. Mokkapati, A. Polman, and K. R. Catchpole, "Asymmetry in photocurrent enhancement by plasmonic nanoparticle arrays located on the front or on the rear of solar cells," Appl. Phys. Lett. **96**(3), 033113 (2010).
18. S. Pillai, F. J. Beck, and K. R. Catchpole, "The effect of dielectric spacer thickness on surface plasmon enhanced solar cells for front and rear side depositions," (submitted).
19. Z. Ouyang, S. Pillai, F. J. Beck, O. Kunz, S. Varlamov, K. R. Catchpole, P. Campbell, and M. A. Green, "Effective light trapping in polycrystalline silicon thin-film solar cells by means of rear localized surface plasmons," Appl. Phys. Lett. **96**(26), 261109 (2010).
20. A. Centeno, J. Breeze, B. Ahmed, H. Reehal, and N. Alford, "Scattering of light into silicon by spherical and hemispherical silver nanoparticles," Opt. Lett. **35**(1), 76–78 (2010).
21. Lumerical FDTD Solutions, *www.lumerical.com*.
22. P. B. Johnson, and R. W. Christy, "Optical Constants of the Noble Metals," Phys. Rev. B **6**(12), 4370–4379 (1972).
23. M. J. Keevers, and M. A. Green, "Absorption edge of silicon from solar cell spectral response measurements," Appl. Phys. Lett. **66**(2), 174–176 (1995).
24. E. D. Palik, *Handbook of Optical Constants of Solids* (Academic Press, New York, 1998).
25. T. L. Temple, G. D. K. Mahanama, H. S. Reehal, and D. M. Bagnall, "Influence of localized surface plasmon excitation in silver nanoparticles on the performance of silicon solar cells," Sol. Energy Mater. Sol. Cells **93**(11), 1978–1985 (2009).
26. K. R. Catchpole, and A. Polman, "Plasmonic solar cells," Opt. Express **16**(26), 21793–21800 (2008).
27. S. Mokkapati, F. J. Beck, R. de Waele, A. Polman, and K. R. Catchpole, "Resonant nano-antennas for light trapping in plasmonic solar cells," (submitted).
28. J. A. Dionne, E. Verhagen, A. Polman, and H. A. Atwater, "Are negative index materials achievable with surface plasmon waveguides? A case study of three plasmonic geometries," Opt. Express **16**(23), 19001–19017 (2008).
29. L. Novotny, "Effective wavelength scaling for optical antennas," Phys. Rev. Lett. (2007).
30. E. Cubukcu, and F. Capasso, "Optical nanorod antennas as dispersive one-dimensional Fabry-Perot resonantors for surface plasmons," Appl. Phys. Lett. **95**(20), 201101 (2009).
31. J. D. Jackson, *Classical Electrodynamics*, 3 ed. (John Wiley and Sons, Inc., New York, 1999).

1. Introduction

It has been over a century since Mie first described the scattering of light from a sphere in a homogeneous medium [1], and yet the scattering behavior of metal nanoparticles is still the subject of active investigation. When a scattering structure is in the vicinity of an interface, light will be preferentially scattered into the medium with the highest optical density. This can be employed to couple incident light into underlying substrates, which has implications for a number of applications, including light management in photovoltaics and photodetectors [2]. The challenge then is to optimize the in-coupling of scattered light to trapped modes within a substrate. Due to the presence of the interface, symmetry is broken and the calculation of the resultant fields becomes more complex. Bobbert and Vlieger [3] solved the problem of a spherical scatterer near an interface, incorporating both Mie theory and the work of Weyl [4]. Like Mie theory, the calculation results in the complete field distribution but, apart from a few cases, needs to be solved numerically. Over the last few decades, access to increased computer power and memory has allowed 3D predictive modeling to be used to solve scattering problems with arbitrary geometries on absorbing substrates. This has lead to the identification of trends in the scattering behaviour of nanostructures [5–7], as well as device optimization [8]. However, for the purposes of achieving a physical understanding of nanoparticle scattering and coupling to a substrate, the simplified case of a dipole above an interface has been invoked by many authors.

Stuart and Hall [9], and later Soller and Hall [10], used classical dipole radiation theory to model the coupling of scattered light into a Si based waveguiding structure. They then extended this to show that a scattering array of random Ag nanoparticles could be described as interacting dipoles [11]. Later on, a non-interacting dipole model was used to investigate the absorption enhancement in Si on insulator solar cells, sensitized with similar arrays of Ag particles [12,13]. It was then demonstrated that light scattered by plasmonic Au particles, on the front of Si substrates, can enhance and *suppress* absorption in the substrate [14]. Here, the quasi-static approximation of particle scattering [15] was invoked, and the wavelength-dependent enhancement and suppression of the absorption was attributed to interference effects. The authors showed that at wavelengths where suppression occurred, light was scattered out of phase with respect to the incident light, due to the phase associated with the

#138671 - $15.00 USD Received 29 Nov 2010; revised 21 Jan 2011; accepted 21 Jan 2011; published 4 Feb 2011

polarisability of the particle. More recently, we investigated the coupling of light into optically dense substrates for light trapping applications in solar cells, by employing finite-difference time-domain (FDTD) calculations in conjunction with an effective dipole model, based on the input/output formalism developed by Mertz [16]. Here, we found that increased coupling occurred when the effective dipole moment was excited close to the semiconductor interface [7]. This lead to design criteria for efficient coupling with the substrate; namely that the particle shape should be chosen to have a centre of mass close to the interface, and that the thickness of the spacer layer, separating the particle from the semiconductor, should be minimized. Additionally, we have demonstrated that the strength of the scattering cross-section of Ag nanoparticles is determined by the strength of the electric field driving the plasmonic resonance, which also varies with spacer layer thickness and is different for front and rear-located nanoparticles, as expected from the dipole approximation [17].

Nonetheless, the dipole model cannot account for all observed scattering behavior. Rear-located particles on ultra-thin spacer layers (less than 10 nm thick) have anomalously high scattering cross-sections, which increase rapidly as the thickness of the spacer layer is reduced: up to twice as large as those of particles on 10 nm spacer layers [17]. This has since been experimentally verified, with larger photocurrent enhancements occurring at long wavelengths for thin Si solar cells, sensitized with rear-located Ag nanoparticles [18,19].

Both references 17 and 18 demonstrate that small reductions in the spacer layer thickness below 10 nm can dramatically increase the strength of the scattering resonance for rear-located particles. Likewise, Hagglund [6], and later Centeno [20], show that the transmission spectra for light coupled into Si substrates due to scattering from front-located, disk-shaped particles, changes markedly depending on the proximity to the substrate for thin spacer layers.

In this paper, we provide an understanding of the key physical mechanisms behind scattering from plasmonic nanoparticles on high-index substrates. We demonstrate the excitation of different types of resonant modes on disk-shaped nanoparticles using FDTD modeling, with the near field concentrated in either the air or the substrate. The observed resonances are attributed to dipole-like free space modes, and resonant surface plasmon polariton (SPP) excitations at the particle/substrate interface, respectively. We compare the scattering behavior of finite sized particles on spacer layers of different thicknesses with ideal dipoles, to investigate the validity of the dipole model for these types of resonant SPP modes. For spacer layer thicknesses which are of interest for light management applications, dipole-like scatterers have cross-sections reduced by roughly 80% due to the presence of the high-index substrate. However, finite particles that can support resonant SPP modes scatter up to 50% *more* strongly when in direct contact with the substrate. From this we demonstrate that the anomalous enhancement in scattering for rear-located particles can be attributed to the type of mode excited at the Ag/substrate interface. This has implications for designing scattering nanostructures for light trapping applications.

2. Simulations

To investigate the resonant plasmonic modes excited on disk-shaped nanoparticles, FDTD numerical simulations were performed. A single, Ag disk on a semi-infinite Si substrate was modelled using the FDTD solutions package from Lumerical [21]. The nanoparticle was separated from the Si by a SiO_2 spacer layer of varying thickness. The simulation volume was terminated by perfectly-matched-layer boundary conditions. As illustrated in the inset in Fig. 1(a), radiation from the normally incident source was propagated from the air region to the substrate, corresponding to nanoparticles on the front of the Si, or from the substrate to air, corresponding to nanoparticles on the rear. For particles on the rear, the source is in the Si, 50 nm from the interface, to minimise the amount of light absorbed in the Si before reaching the particle. The incident electric field was linearly polarised. This does not restrict our analysis of the results as the particles are rotationally symmetric and therefore the scattering is polarisation independent. The dielectric functions of the materials were modelled using a Drude model for Ag, fitted to optical data from Johnson and Christy [22], and a Drude-

#138671 - $15.00 USD Received 29 Nov 2010; revised 21 Jan 2011; accepted 21 Jan 2011; published 4 Feb 2011

Lorentz model for Si, fitted to data from Keevers and Green [23]. The refractive index of SiO_2 was taken from data from Palik [24].

We are primarily interested in the wavelength dependent scattering behaviour of the nanoparticle; namely how much light is scattered and what fraction of the scattered light is coupled into the Si substrate. To investigate this we calculate the normalised scattering cross-section and the coupling efficiency of the nanoparticle, as described below.

The total power scattered by the nanoparticle was calculated by integrating the Poynting vector of the scattered field over a closed surface surrounding the particle. The normalised scattering cross-section, Q_{scat}, was then calculated by dividing the total scattered power by the incident source irradiance, and normalising the result to the cross-sectional area of the particle. The scattered power was evaluated separately in the air and in the substrate. In the Si the surface over which the integration is performed is 100 nm from the interface; for wavelengths above 500 nm, less than 10% of the scattered light is absorbed in the Si before reaching the monitor. This allows the fraction of scattered light coupled into the substrate (F_{subs}) to be calculated by dividing the scattered power in the Si by the total scattered power.

3. Identification of resonances

Figure 1(a) shows the calculated Q_{scat} spectra for a 100 nm diameter, 50 nm tall, disk-shaped Ag nanoparticle, separated from a Si substrate by a SiO_2 spacer layer of thickness, t = 0, 5 or 20 nm. Spectra are shown for particles on the front, illuminated surface of the Si (light incident from the air, crosses) and for rear-located particles (light incident from the Si, solid lines).

Figure 1(a) clearly shows two distinct scattering peaks for each Q_{scat} spectra, labelled R1 and R2, corresponding to resonant plasmonic modes. Evidence of these modes has been previously demonstrated in experimental transmission spectra of Ag particles on glass substrates. In that work, both the short-wavelength mode corresponding to R1, and the main plasmonic resonance corresponding to R2 were observed [25]. For both front- (crosses), and rear-located particles (solid lines), the R2 resonance wavelength, λ_{R2}, red-shifts by up to 416 nm as the spacer layer thickness is decreased from 20 to 0 nm. However, the R1 resonance peak wavelength, λ_{R1}, does not shift significantly.

Since the Si is strongly absorbing at short wavelengths, the strength of the normalised scattering cross-section at the R1 resonance, $Q_{scat}(\lambda_{R1})$, cannot be accurately calculated, especially for rear-located particles. However, we can calculate the strength of the normalised scattering cross-section at the R2 resonance, $Q_{scat}(\lambda_{R2})$. This increases as the spacer layer thickness increases for front-located particles, in agreement with previously reported results [17]. Additionally, anomalous enhancement of the scattering cross-section is observed for rear-located particles on ultra-thin spacer layers of t = 5 nm, which increases significantly for particles directly on the Si, as reported in ref 17. To date, the physical mechanism behind this enhancement has not been identified.

Figure 1(b) shows the wavelength dependent coupling efficiency, F_{subs}, for front-located nanoparticles, defined as the fraction of the total light scattered that is scattered into the Si substrate. Similar spectra are obtained for rear-located particles, as F_{subs} is independent of illumination direction for symmetrical particle shapes [17]. At wavelengths less than 400 nm, F_{subs} rapidly reduces for all particles due to absorption in the Si. In order to investigate F_{subs} at short wavelengths around the R1 resonance, the coupling efficiency is also calculated for a particle directly on a non-absorbing, high-index substrate, with refractive index n = 3.5 (dotted line, black circles). This clearly shows that there is a strong reduction in the coupling efficiency at wavelengths corresponding to the R1 resonance: from over 96% at long wavelengths to around 60%. Significantly, at wavelengths corresponding to the R2 resonance the coupling efficiency remains high, despite the presence of the resonant mode. However, as the spacer layer thickness is increased, the overlap of the near field of the resonant mode with the substrate reduces, and hence F_{subs} decreases, in agreement with previously reported results [26].

#138671 - $15.00 USD Received 29 Nov 2010; revised 21 Jan 2011; accepted 21 Jan 2011; published 4 Feb 2011

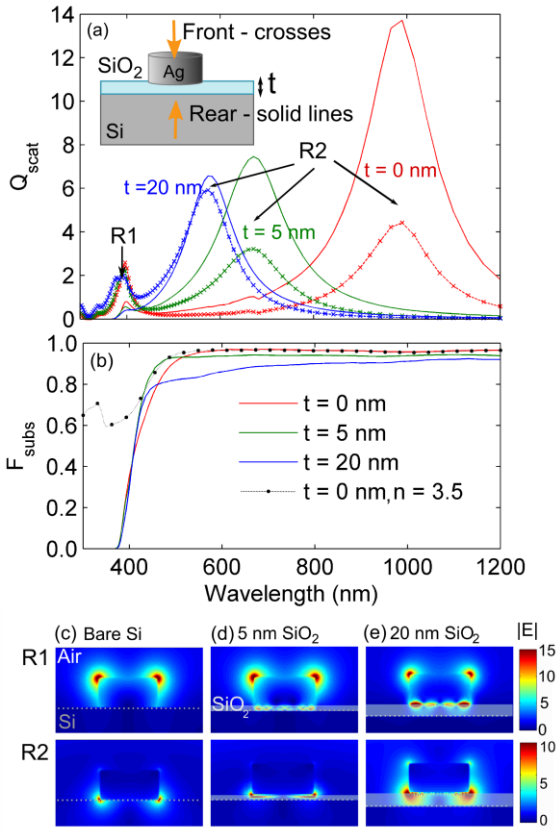

Fig. 1. (a) Calculated normalized scattering cross-section spectra (Q_{scat}) of a 100 nm diameter, 50 nm tall, Ag disk on the front (crosses), or rear (solid line), of a Si substrate. The particle is either directly on the Si surface (t = 0 nm) or on thin SiO_2 spacer layers of thickness, t = 5 nm and t = 20 nm. (b) The coupling efficiency (F_{subs}) for the particles on the front of a Si substrate, calculated as the fraction of the scattered light scattered into the substrate. Data is also shown for a particle directly on the surface of a non-absorbing substrate with refractive index, n = 3.5 (dashed lines, black circles). (c-e) The electric field profiles (|***E***|) calculated over a plane bisecting the nanoparticle, with light incident from the air. Data is shown at the resonance wavelengths marked in (a), where (c) R1 λ_{R1} = 396 nm, and R2 λ_{R2} = 990 nm for particles on bare Si, (d) R1 λ_{R1} = 396 nm, and R2 λ_{R2} = 671 nm for t = 5 nm, and (e) R1 λ_{R1} = 388 nm, and R2 λ_{R2} = 574 nm for particles on a 20 nm thick oxide.

Figures 1(c-e) show the electric field profiles for front-located particles at wavelengths corresponding to the two resonance peaks marked in Fig. 1(a). Data is shown for particles on (c) bare Si, and with spacer layers of thicknesses (d) t = 5 nm, and (e) t = 20 nm. The magnitude of the electric field, |**E**|, is calculated over the plane parallel to the direction of polarization and perpendicular to the interface, bisecting the particle. Similar field profiles are observed for rear-located particles; however the R1 mode is much weaker due to absorption of light in the substrate before reaching the particle. At $\lambda_{R1,}$ for all spacer layer thicknesses, the field plots clearly show that the electric field is concentrated on the air/Ag interface, at the edges of the particle. For particles on a spacer layer (d-e) we also see field concentration in the oxide layer. Conversely at λ_{R2}, the field is concentrated on the Ag/Si or Ag/SiO_2 interface at the edges of the particle. Similar field localization at the Si interface has been observed by Hagglund for Au nanodisks [6], who attributed the behavior to two asymmetric dipoles, localised at the air and substrate side of the particle, dominated by the substrate dipole. For the R2 mode, the near field overlaps with the substrate, which has been shown to result in more efficient coupling with the Si [7], as is evident from the F_{subs} spectra in Fig. 1(b). Conversely

#138671 - $15.00 USD Received 29 Nov 2010; revised 21 Jan 2011; accepted 21 Jan 2011; published 4 Feb 2011

for the R1 mode, the near field does not overlap significantly with the substrate, and consequently in-coupling is reduced.

4. Resonant SPP modes

To understand the origin of these different plasmonic modes, it is insightful to view the nanoparticle resonances as being due to confined surface plasmon polaritons (SPPs) on the individual Ag/Si and Ag/SiO_2 interfaces. In this interpretation, reflections of the SPPs at the nanoparticle edges give rise to resonances. To first approximation, these are expected to occur when the diameter of the particle is equal to $^{m}/_{2}\ \lambda_{spp} + l_{\varphi}$, where λ_{spp} is the wavelength of the SPPs on an infinitely extended film, l_{φ} is an additional term, with units of length, to account for the phase shift introduced by reflection at the sides of the particle [27–30], and m is an integer.

We consider the SPPs that can be excited at the interfaces of a thin, infinitely extended, Ag film on a Si substrate. Dispersion relations, $\lambda_0(\lambda_{spp})$, were calculated for SPPs on two different 1D multilayer structures: 1) a 50 nm thick Ag film between two semi-infinite half spaces of air and Si, corresponding to a particle on a bare Si substrate, and 2) including a 20 nm SiO_2 layer between the Ag and the Si, representing the spacer layer. The SPP wavelengths were obtained by determining the poles of the transfer matrix of the 1D multilayer stack [28]. Two SPP modes $\lambda_{spp,air}$ and $\lambda_{spp,sub}$ exist, with fields localized predominantly at either the air/Ag or Ag/substrate interfaces, respectively. From these dispersion relations, we can predict the resonance wavelength, λ_{Rj}, for a given resonator length, d, at which $d \approx {}^{m}/_{2}\lambda_{spp}$, assuming that l_{φ} is small [29].

We then compare this model to the response of Ag stripes of varying widths, calculated using 2D FDTD simulations. Here the incident light is polarized parallel to the width of the stripe, so that d corresponds to the particle diameter in the 3D case, and all other simulation parameters are the same, as described above. Studying the 2D case allows a more direct comparison with the 1D dispersion relations. Although this is a simplification of the particle geometry, similar scattering behavior is observed. As for the 3D case shown in Fig. 1(a), 2 separate resonance peaks occur in the Q_{scat} spectra of 2D stripes with d = 100 nm. For stripes on bare Si, the peak positions of the modes are shifted by only ~6% compared to the 3D case of disks.

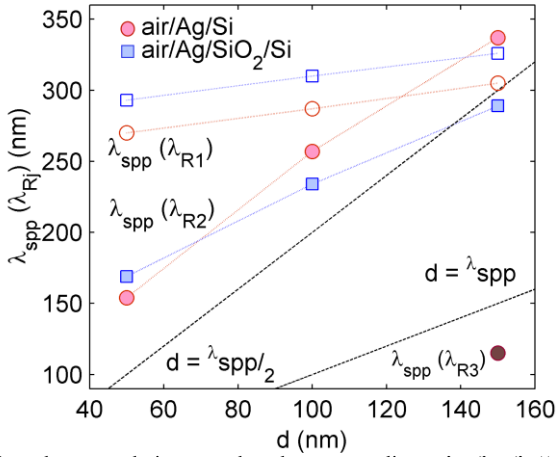

Fig. 2. The surface plasmon polariton wavelength corresponding to λ_{Rj} ($\lambda_{spp}(\lambda_{Rj})$) plotted against stripe width (d). For R1, the wavelength of the SPPs excited at the air/Ag interface is shown ($\lambda_{spp}(\lambda_{R1})$), hollow shapes), while for R2 ($\lambda_{spp}(\lambda_{R2})$), light filled shapes) and R3 ($\lambda_{spp}(\lambda_{R3})$), dark filled shape) the wavelength of the SPPs at the Ag/substrate interface is shown. The conditions $d = {}^{1}/_{2}\ \lambda_{spp}(\lambda_{R2})$, and $d = \lambda_{spp}(\lambda_{R3})$ are plotted for comparison.

Figure 2 shows the SPP wavelength (calculated from the 1D dispersion relations) corresponding to the free space wavelength at which resonance occurs (obtained from the 2D

#138671 - $15.00 USD Received 29 Nov 2010; revised 21 Jan 2011; accepted 21 Jan 2011; published 4 Feb 2011

FDTD simulations) for the different modes, $\lambda_{spp}(\lambda_{Rj})$, plotted against the stripe width, d. Here, we plot $\lambda_{spp,air}$ for R1 (which has strongest fields at the Ag/air interface) and $\lambda_{spp,sub}$ for R2 and R3 (with field localised in the substrate). Data is shown for the case of a stripe on a bare Si substrate (circles) and with a 20 nm SiO_2 spacer layer present (squares). For large stripe widths of d = 150 nm, directly on the Si, a third resonance occurs at λ_{R3} (dark filled circle). This mode is also seen for 3D disk-shaped particles with diameters larger than 150 nm (not shown).

From Fig. 2 we can clearly see that there is a correlation between $\lambda_{spp}(\lambda_{R2})$ and d, consistent with the excitation of resonant SPP modes when $^1/_2\ \lambda_{spp}(\lambda_{R2}) \approx d$. The condition d = $^1/_2\ \lambda_{spp}(\lambda_{R2})$ is plotted for comparison. Deviations from this relationship are attributed to wavelength-dependent phase shifts introduced by reflection at the edges of the Ag stripe [27–30], which are not accounted for in the calculation of the 1D dispersion relations. The propagation lengths of the calculated SPP modes are at least a factor of 30 times larger than d at $\lambda_{spp}(\lambda_{R2})$ for all cases. Similarly, for the R3 mode excited for the stripe width d = 150 nm, directly on Si, $\lambda_{spp}(\lambda_{R3}) \approx$d. Again, differences are attributed to phase shifts on reflection from the edges of the stripe. For the R3 mode the propagation length of the calculated SPP mode is on the order of the particle diameter at λ_{R3}.

It can also be seen from Fig. 2 that $\lambda_{spp}(\lambda_{R1})$ does not correlate strongly with the stripe width. Instead, we attribute the R1 mode to localised surface plasmon resonances at the top of the particle, in the air region. Here, we should recall that at λ_{R1} some concentration of the near field was observed at the Ag/SiO_2 interface in Fig. 1(d) and (e). Interestingly, for particles on an oxide, the SPP excitation at the Ag/SiO_2 interface has a wavelength, $\lambda_{spp,sub}$ (λ_{R1}), on the order of the stripe width (data not shown). This suggests that the electric field concentration at the Ag/SiO_2 interface at λ_{R1} may be due to non-resonant SPPs. For particles directly on Si, $\lambda_{spp,sub}$ (λ_{R1}) at the Ag/Si interface is at least a factor of 5 larger than the particle width, and at this wavelength, no field concentration is seen in the substrate at λ_{R1} in Fig. 1(c). This suggests that for particles directly on the interface the particles are too small to support SPPs excited at λ_{R1}.

From the results presented so far, we attribute the plasmonic modes observed on Ag stripes, on Si substrates, to two different types of resonances. At λ_{R1} the resonance can be interpreted as a localised surface plasmon resonance in air, while at λ_{R2} and λ_{R3} the modes behave like geometric resonances of SPPs at the Ag/substrate interface.

To determine whether geometrical resonances of SPP modes are excited on 3D particles, we look at the near field of a 150 nm diameter, Ag disk on a Si substrate, obtained from 3D FDTD simulations, as described aboveFig. 3 shows the real part of the component of the electric field in the direction of polarisation, Re($\mathbf{E}_x$), plotted over a plane parallel to the direction of polarisation, and perpendicular to the interface, bisecting the particle. As in the 2D case for d = 150 nm, three scattering resonances are observed. In Fig. 3 the fields are plotted at the free space wavelengths corresponding to the three resonances: (a) λ_{R1} = 368 nm, (b) λ_{R2} = 1274 nm and (c) λ_{R3} = 744 nm. The field profiles clearly show evidence of resonant SPP modes at (b) λ_{R2} and (c) λ_{R3}. In Fig. 3(b) the field at the Ag/Si interface corresponds to a standing wave with a half wavelength equal to the particle length, while at λ_{R3} in (c) the field corresponds to a standing wave with a wavelength equal to the particle length. This is illustrated in the insets, which show schematics of the field at the Ag/Si interface. The SPP wavelengths were determined from the distances between nodes to be 314 nm at λ_{R2} from Fig. 3(b), and 102 nm at λ_{R3} from (c), which are consistent with the resonance conditions $^1/_2\ \lambda_{spp}(\lambda_{R2}) \approx d$ and $\lambda_{spp}(\lambda_{R3}) \approx d$, respectively.

#138671 - $15.00 USD Received 29 Nov 2010; revised 21 Jan 2011; accepted 21 Jan 2011; published 4 Feb 2011

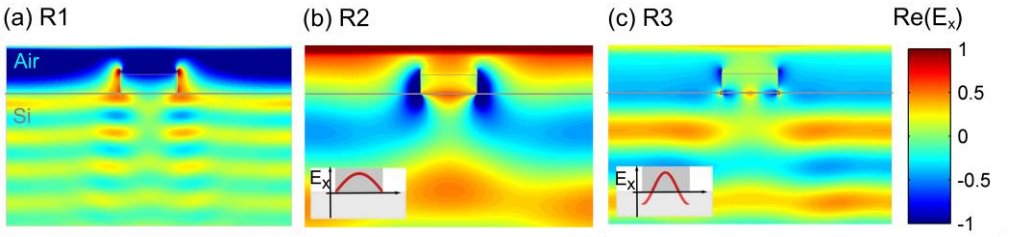

Fig. 3. Field profile of the real part of the component of the electric field vector in the direction of polarisation ($Re(E_x)$) calculated from 3D FDTD simulations. Data is shown for a 150 nm diameter, 50 nm tall, disk-shaped particle on a bare Si substrate with light incident from the air. The plots are shown at the free space resonance wavelengths, (a) λ_{R1} = 368 nm, (b) λ_{R2} = 1274 nm and (c) λ_{R3} = 744 nm. Insets in (b) and (c) show a schematic representation of $Re(E_x)$ at the Ag/Si interface.

We can conclude that two different types of modes can be excited on 3D, disk-shaped Ag particles, on Si substrates. The short wavelength R1 mode can be attributed to a dipole-like excitation in air, while the longer wavelength R2 and R3 modes can be associated with geometrical resonances of SPP modes at the interface between the particle and the substrate.

5. Comparison with the dipole model

To investigate the trends in scattering behaviour observed for the types of resonant SPP modes identified above, we compare $Q_{scat}(\lambda_{R2})$ to predictions from the dipole model. To compare with the calculated $Q_{scat}(\lambda_{R2})$ for finite particles, we can calculate the scattering cross-section of a horizontally orientated dipole, σ, separated from a Si substrate by a SiO_2 spacer layer of varying thickness. The scattering cross-section of a dipole is defined as the ratio of the scattered power and the incident irradiance, and can be calculated as [16]

$$\sigma = \frac{2\pi}{\lambda}\Im m[\alpha_m]I_d, \qquad (1)$$

where α_m is the effective polarisability, which includes modifications to the polarisability of the dipole due to the proximity to the substrate, and the effects of the scattered field reflected at the interface on the radiative damping. From Eq. (1), the scattering cross-section of an ideal dipole varies as a function of the intensity of the electric field driving the oscillation, I_d. The extent to which this relationship holds for finite, disk-shaped, Ag nanoparticles can be determined by comparing Q_{scat} and I_d. Here we use a simple model to calculate the driving field intensity at the position of the particle, as described in Ref [17]. For front-located particles, the driving field is equal to a superposition of the field incident in air, and the portion of the field that is back reflected at the interface. For rear-located particles, the driving field is equal to the portion of the field, incident in the Si, which is transmitted at the interface.

The incident fields in the air and in the Si are normalized so that the incident irradiance, given by [31] $I = {}^1/_2\varepsilon_0 c n_{in}|\mathbf{E}_i|^2$, is equal in each medium, where n_{in} the refractive index of the incident medium. The ratio of the incident fields in the air and in the Si is then equal to $\sqrt{n_{Si}}$. The driving field intensity, I_d, is given by the square of the driving field, normalized to the incident intensity in air.

In Fig. 4(a), the strength of the scattering cross-section at the R2 resonance, $Q_{scat}(\lambda_{R2})$, calculated for a 100 nm diameter, disk-shaped, Ag nanoparticle on a Si substrate with a SiO_2 spacer layer, is plotted against different thicknesses of SiO_2, t. Here, $Q_{scat}(\lambda_{R2})$ is normalized to the scattering cross-section of a similar disk in free space, Q^{∞}_{scat}. In Fig. 4(b), the cross-section of a horizontally orientated dipole, normalized to the cross-section of a dipole in free space, σ/σ^{∞}, is calculated for the same substrate layer geometry as in part (a). Here, σ/σ^{∞} is calculated at wavelengths corresponding to λ_{R2} for the disks in Fig. 4(a). Data is shown for particles illuminated on the front of a Si substrate (blue, circles), and on the rear (red, squares). The intensity of the electric field driving the resonance, I_d, calculated at wavelengths

#138671 - $15.00 USD Received 29 Nov 2010; revised 21 Jan 2011; accepted 21 Jan 2011; published 4 Feb 2011

corresponding to λ_{R2} for each value of t, is also plotted on both graphs (solid lines). As the driving field intensity for a scatterer in free space would be equal to the incident intensity, I_d can be interpreted as the change in the driving field intensity due to the presence of the substrate.

The inset in Fig. 4(b) shows the relative efficiency of excitation, η, calculated as σ/σ^{∞} divided by I_d. For dipoles, η can be identified as the change in the polarisability of the dipole due to the presence of the substrate, plotted against t. The presence of the substrate results in a reduced polarisability, as the dipole decay rate is modified due to the interaction of the dipole with the scattered field that is back-reflected in the substrate [16]. Hence, for dipoles, η is less than 1 for all values of t shown. Additionally, as it is only dependent on the local dielectric environment of the particle, η is equal for front and rear-located dipoles.

For finite, disk-shaped particles, η is calculated as $Q_{scat}(\lambda_{R2}) / Q^{\infty}_{scat}$ divided by $I_{d.}$ Since the polarisability of finite particles supporting resonant SPPs is not well defined, this can no longer be associated with a change in polarisability. Instead, we can identify η as the efficiency of the excitation of resonant scattering modes in the vicinity of a substrate, relative to the efficiency of the excitation of resonant scattering modes in free space. Here we note that in free space we are exciting a different type of resonant scattering mode, as we will discuss below.

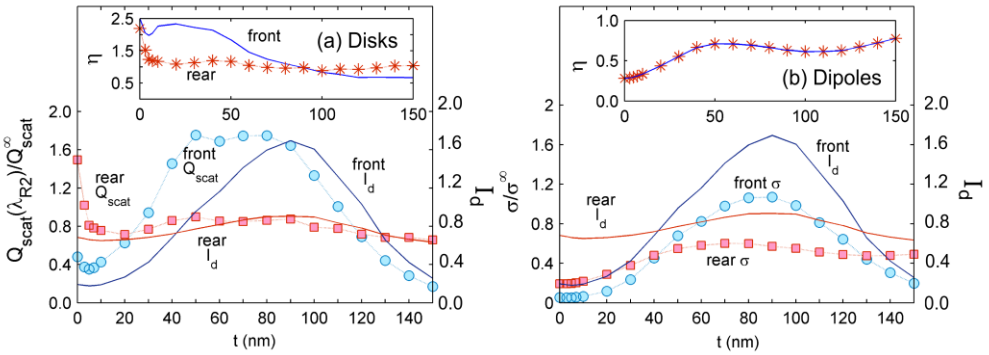

Fig. 4. (a) Strength of the scattering cross-section at the R2 resonance ($Q_{scat}(\lambda_{R2})$) for a 100 nm diameter, disk-shaped, Ag nanoparticle, on a Si substrate, normalised to the scattering cross-section of a similar disk in free space (Q^{∞}_{scat}) for different thicknesses of SiO_2, from t = 0-150 nm. (b) Strength of the scattering cross-section for a horizontally orientated dipole on a Si substrate for different thicknesses of SiO_2 spacer layer, normalised to the cross-section of a dipole in free space (σ/σ^{∞}). The cross-section is calculated using the Mertz formulation [16], at wavelengths corresponding to λ_{R2} for the disks in part (a). For both parts of the figure, data is shown for particles on the front (circles, blue) and rear (squares, red) of the substrates. The intensity of the electric field driving the resonance (I_d) normalised to the incident radiation, calculated using a simple model for a multilayered substrate described in ref [17] is also plotted (solid lines). The insets show the relative efficiency of excitation (η), calculated as the normalised scattering cross-section divided by intensity of the driving field, for front (stars, red) or rear-located scatterers (blue, solid line).

From Fig. 4, we find that while the driving field is important in determining the strength of the cross-section of both dipoles and finite particles, there are some clear differences in the efficiency of excitation.

Firstly, from the inset in Fig. 4(a), asymmetry in η is observed for finite particles on the front and on the rear of substrates. We attribute this to the fact that the driving field is calculated at the interface, in the absence of the particle. For a disk-shaped particle this simplification does not take into account the finite extent of the particle and the complex interaction between the incident light and the particle near field, which would be dependent on the direction of illumination.

Secondly, once the overlap of the particle near-field with the Si substrate is significant (t < 80 nm), the efficiency of the excitation *increases* for finite particles in the vicinity of a Si

#138671 - $15.00 USD Received 29 Nov 2010; revised 21 Jan 2011; accepted 21 Jan 2011; published 4 Feb 2011

substrate, in contrast to the dipole case. This is attributed to changes in the nature of the resonant scattering mode in the vicinity of a high-index substrate. In free space, the particle scattering resonance is dominated by a localised surface plasmon resonance. The presence of an interface breaks the symmetry, and the mode is localised at the interface with the substrate. Now the resonance is dominated by geometrical resonances of SPPs confined to the volume of the particle. This changes the efficiency of the excitation, and introduces increased asymmetry for front and rear-located particles.

Finally, η increases rapidly for finite particles on ultra-thin spacer layers; to a value of 2.5 on the front and 2.2 on the rear at t = 0 nm. This means that for finite, rear-located particles, directly on the Si substrate, $Q_{scat}(\lambda_{R2})$ is 1.5 times *larger* than the strength of the scattering resonance in free space. In contrast, for spacer layer thicknesses of t = 0-20 nm, which are of interest for light management applications due to high coupling efficiencies, the cross-section of a dipole is *less* than 20% of the free space case, as both I_d and η are less than 1.

In order to investigate the sensitivity of λ_{R2} and $Q_{scat}(\lambda_{R2})$ to small changes in the spacer layer thickness, the electric fields due to the R2 mode were calculated for a 100 nm diameter, disk-shaped particle, with either no spacer layer, with an ultra-thin spacer layer of 5 nm, and with t = 20 nm. To calculate the field due to the resonant mode, 3D simulations were run with and without a particle present. The electric field was calculated over the plane parallel to the direction of polarisation and perpendicular to the interface, bisecting the particle, as in Fig. 1(c-e). The magnitude of the electric field due to the resonant mode, $|\mathbf{E}_{MODE}|$, was then determined by subtracting the field without the particle present, from the field with the particle.

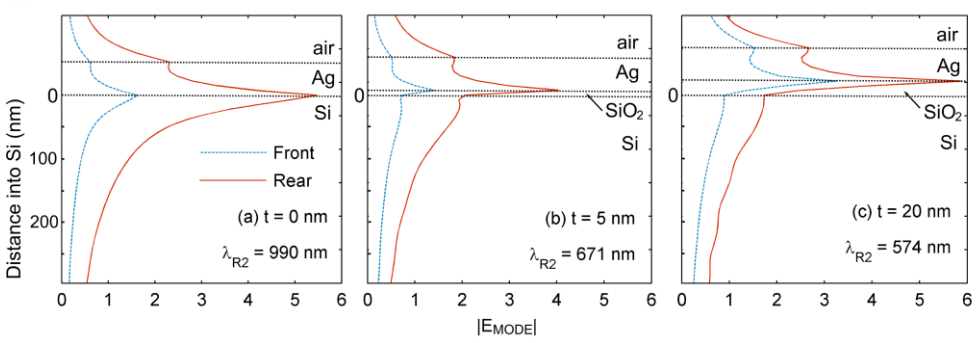

Fig. 5 Magnitude of the electric field due to the resonant mode at λ_{R2} ($|E_{MODE}|$) normalized to the incident field for a 100 nm diameter, disk-shaped nanoparticle on a Si substrate. Data is shown for particles on the Si substrate with (a) t = 0 nm and λ_{R2} = 990 nm, (b) t = 5 nm with λ_{R2} = 671 nm, and (c) t = 20 nm with λ_{R2} = 574 nm. The results are plotted perpendicular to the substrate, at the centre of the particle.

Figure 5 shows the magnitude of the field due to the R2 mode, $|\mathbf{E}_{MODE}|$, for (a) no spacer layer, (b) t = 5 nm, and (c) t = 20 nm. The results are plotted perpendicular to the interface, at the centre of the particle. It is clear that high field gradients exist close to the particle. In Fig. 5(a) the intensity maximum occurs at the Ag/Si interface, while in (b) and (c) the field maximums occur at the Ag/SiO_2 interface. For particles on an oxide, the field is localised on the Ag/SiO_2 interface and the field intensity is concentrated in the thin SiO_2 layer. For particles directly on the Si, the mode is excited along the Ag/Si interface, resulting in high field intensities in the Si that extend into the substrate.

From this we can see that for particles on or very close to the Si (within 5 nm), the excitation changes from an Ag/SiO_2 mode to an Ag/Si mode. This corresponds to a rapid increase in the efficiency of excitation for nanometre changes in t, especially for rear-located particles. From Fig. 5, modes excited at or very close to the Ag/Si interface have a larger spatial overlap of the mode with the Si. This allows them to couple efficiently to incident light in the Si, and gives rise to large enhancements in $Q_{scat}(\lambda_{R2})$ of up to 87% as the spacer layer is reduced from 5 to 0 nm. From this, we attribute the anomalously high scattering cross-

#138671 - $15.00 USD Received 29 Nov 2010; revised 21 Jan 2011; accepted 21 Jan 2011; published 4 Feb 2011

sections observed for rear-located particles on ultra-thin spacer layers to the type of resonant SPP modes excited at the Ag/substrate interface.

It is clear that for plasmonic particles, the excitation efficiency as well as the driving field needs to be optimised to achieve strong scattering in the vicinity of a high-index substrate, and this can be achieved by ensuring a large near-field overlap with the substrate.

6. Conclusion

We provide key physical insights into scattering from nanostructures on high-index substrates, beyond the dipole model. At short wavelengths, a dipole-like, free space resonance dominates, while at long wavelengths, the resonance can be attributed to the excitation of resonant surface plasmon polariton modes at the particle/substrate interface. These types of resonant modes have increased excitation efficiencies when the particle near-field overlaps significantly with the substrate. This can lead to very high scattering cross-sections for particles that support resonant SPP modes at the Ag/substrate interface; up to 7.5 times larger than that of a dipole with an equivalent free space resonance. This has implications for designing scattering nanostructures, namely that to ensure strong scattering and efficient coupling, especially from rear-located structures, there should be a large near field overlap with the substrate. Due to high scattering cross-sections and coupling efficiencies these modes have the potential to provide effective light trapping for photodetectors and photovoltaics devices.

Acknowledgements

The research at the ANU is financially supported by the Australian Research Council and the EU FP7 PRIMA project. Work at AMOLF is part of the research program of the Foundation for Fundamental Research on Matter (FOM) which is financially supported by NWO. It is also supported by GCEP. The Authors would also like to acknowledge the Australian National University Supercomputer facility for supplying computational resources.

#138671 - $15.00 USD Received 29 Nov 2010; revised 21 Jan 2011; accepted 21 Jan 2011; published 4 Feb 2011